Electronic Supplement 1
Estuaries and Coasts

Monitoring vegetation dynamics at a tidal marsh restoration site: Integrating field methods, remote sensing and modeling

Alexandra S. Thomsen, Johannes Krause, Monica Appiano, Karen E. Tanner, Charlie Endris, John Haskins, Elizabeth Watson, Andrea Woolfolk, Monique C. Fountain, Kerstin Wasson*

*corresponding author: Kerstin Wasson, Elkhorn Slough National Estuarine Research Reserve, 1700 Elkhorn Rd, Watsonville, CA 95076, USA; kerstin.wasson@gmail.com, (831)728-2822 x310

SUPPLEMENTARY METHODS & RESULTS

Estimating Vegetated Area Before Degradation and Before Restoration

To quantify baseline conditions at the restoration site, we digitized georeferenced aerial imagery from 1931 in ArcGIS software as vegetated marsh, unvegetated mudflat/basin, and tidal creeks (pixel size = 0.63 m, collected by Western Gulf Oil Co., part of the Fairchild Aerial Surveys, Inc. collection). We calculated the vegetated area in 1931 within the restoration project footprint in ArcGIS. To quantify vegetated area under degraded conditions prior to restoration, we digitized georeferenced UAS imagery from October 2015 in ArcGIS software as vegetated marsh, unvegetated mudflat/basin, tidal creeks, vegetated berms, grassland, and other unvegetated areas which included berms and roads. We calculated the vegetated area prior to restoration as the area in 2015 that had marsh vegetation (including vegetated berms) within the restoration project footprint.

Area Searches for Marsh Vegetation Surviving Construction

During area surveys of the construction zone, we logged points where we found plants on the marsh plain using a handheld GPS (Trimble Juno 3B, Trimble Inc., Sunnyvale, CA), with each point representing the approximate number of plants for each species found within a 1-m diameter area. We used this approach because plants were very sparse and often appeared in clusters. We are fairly certain that the native marsh plants we found were survivors and not new colonists, because surveys were conducted between October 10 and November 13 and these species do not typically germinate until the late winter or early spring (Mayer 1987; Noe and Zedler 2001).

To calculate cover of surviving vegetation found during area searches in the construction zone, we multiplied the estimated number of individuals of each species by the approximate size of an individual of that species. Based on ground truthing during field surveys, we assumed an area of 64 cm^2 for each *Distichlis spicata* individual, 100 cm^2 for *Jaumea carnosa* and *Frankenia salina*, 225 cm^2 for *Salicornia pacifica* and *Spergularia sp*., and 400 cm^2 for unidentified species. When it was difficult to distinguish whether plants in the field were many small individuals or one large one, these approximate area estimates were used to determine the number of individuals to log at each location.

To evaluate conditions under which marsh vegetation survived, we examined these points in relation to the digitized 2015 imagery showing where vegetation existed before construction and an elevation change raster showing the amount of soil added or removed during construction (calculated by subtracting a pre-construction, October 2015 DSM from a post-construction, August 2018 DSM; resolution of these UAS-derived DSMs is shown in Table 1). If vegetation was present in areas that were vegetated in 2015 imagery and that had positive elevation change, we assumed the plants survived soil addition. If vegetation was present in areas of elevation loss that were vegetated in 2015, we assumed the plants survived scraping (soil removal which was undertaken to incorporate formerly high areas like berms into the restored marsh). If vegetation was present within 5 m of those formerly vegetated and scraped areas, we considered those plants as potentially originating from the scraped soil. If plants were found in areas that were unvegetated prior to restoration beyond 5 m of former berms, we included them in estimates of 2018 vegetation cover, but their mechanism of survival is unknown. Upland plants were also included in these initial estimates, but were not assumed to be survivors (prior to construction, soil salinity was far too high for upland plants to survive, so these must have colonized after construction).

The surviving plants were mostly located on former berms or other vegetated areas that had been scraped down to the target elevation of the marsh (2,887 plants; 69.7% of surviving plants) or in areas of soil addition within 5 m of former berms (426 plants; 10.3% of surviving plants). These near-berm plants were assumed to have originated from berm material that was pushed off to the side as the berm was levelled. An additional 445 plants (10.7% of surviving plants) were in areas of soil addition that were formerly vegetated marsh. On average, this third group of plants experienced 30 cm of soil addition (± 16 cm standard deviation). However, this category includes some overlap with vegetation that may have originated from berms, which may explain the high levels of soil addition that some plants appeared to survive. Only 387 plants (not including upland non-natives) were found in formerly unvegetated areas beyond 5 m of former berms.

Transect Monitoring of Vegetation Colonization

The point-intercept method we used to survey percent cover along transects utilized a 50 cm by 50 cm quadrat frame with a grid of strings running across it, creating 16 intercepts where the strings cross. The quadrat was elevated off the ground to prevent damage to marsh vegetation. At each intercept, we dropped a metal rod and recorded all vegetation species that touched the rod. If no living plant touched the intercept rod, the intercept was recorded as “bare.” We calculated percent cover for a given species within each quadrat as the number of intercepts where that species was recorded divided by the total number of intercepts, multiplied by 100. This had the potential to result in percent cover exceeding 100% when calculated for multiple vegetation species combined, which represents canopy layering by the different species.

In our random forest modeling of vegetation cover, we used the following variable selection method to reduce the number of variables to examine and discuss further. We started by running a full model with all nine predictors and then removed one variable at a time, starting with the least important. After each variable was removed, we evaluated model performance based on out-of-bag data (the data not used for model training during one iteration of the subsampling process). We excluded variables when their inclusion did not increase the percentage of variance explained by the model. We also used this variable selection method for modeling UAS-derived vegetation cover.

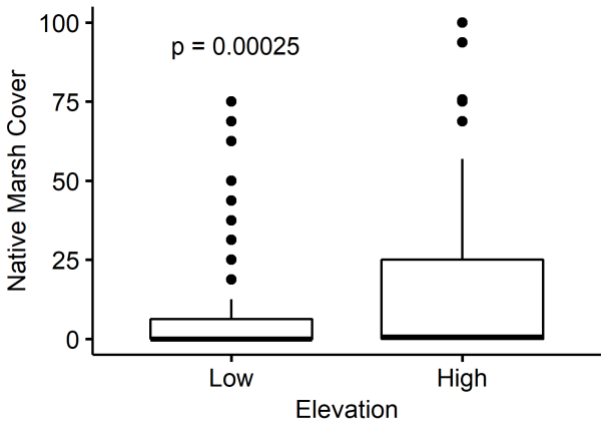

Fig. S1 Percent cover of native marsh species at high (≥1.93 m) and low (<1.93 m) elevation quadrats on 10 transects, August 2019. P-value from one-tailed t-test

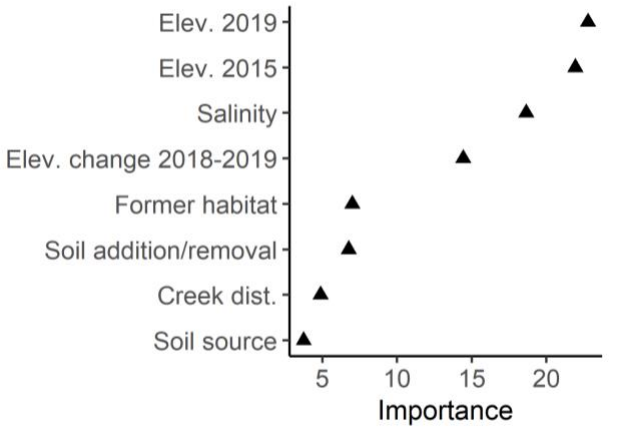

Fig. S2 Importance for variables included in the random forest model of percent cover of native marsh plants surveyed along 10 transects in August 2019. Variable importance is measured as percentage increase in mean squared error when the variable is randomly permuted

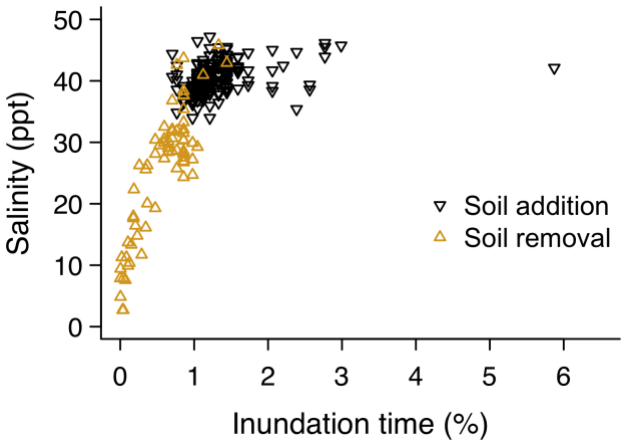

Fig. S3 Relationship between salinity and tidal inundation time in transect quadrats (n = 252)

Characterization of Inundation Across Elevations

To understand how inundation varies across the different elevations at Hester Marsh and influences vegetation patterns, we used ESNERR's permanent water quality monitoring sonde at nearby Vierra Marsh, leveled in to NAVD88, to track water levels every 15 minutes from August 2018 to May 2019. Tide ranges and timing are nearly identical throughout the Elkhorn Slough estuary due to strong tidal forcing, so data from this nearby station were expected to be accurate for Hester Marsh. We confirmed the accuracy by monitoring the areas inundated on several high tides (both in the field and in UAS imagery), determining the elevation ranges of the inundated areas using DSMs, and comparing the inundated elevations with the Vierra tide data. We calculated percent time inundated as total hours a given elevation was inundated divided by total hours recorded by the sonde, multiplied by 100.

We also used tide data to delineate the area receiving tidally-dispersed seeds so we could exclude areas we expected to be dominated by upland plants from site-wide analyses of marsh vegetation colonization. Based on the tidal dispersal mechanism of seeds (Huiskes et al. 1995; Morzaria-Luna and Zedler 2007) and seasonal variation in seed abundance (Mayer 1987), we identified the "main seed dispersal area" as all elevations below the highest tide level that occurred between October 2018 and March 2019.

We also evaluated the influence of tides on the upper marsh boundary by identifying the most landward *Salicornia* plant on each of the five initially-bare western transects (numbered 1-5 in Fig. 1) and the five southern and eastern transects (numbered 6-10 in Fig. 1) that started in existing vegetation outside of the construction zone. We estimated the elevation of each of these plants using an August 2019 DSM, and compared the *Salicornia* elevations with tide levels to examine whether the upper marsh boundary differs between new and existing vegetation. We expected that if the highest tide during the main seed dispersal period (October 2018 to March 2019) was lower than historical king tides, the upper elevational limit of newly-colonized *Salicornia* would be lower than that of previously established *Salicornia*.

The elevation range of Hester Marsh (approximately 1.7 m to 2.3 m) was inundated between 0.0% and 6.2% of the time from August 2018 to May 2019 (Fig. 7d). The highest tide during this period was 2.29 m on August 10, 2018, according to Vierra Marsh tide data. Elevations over 1.95 m were inundated <1.0% of the time. The highest tide during the main seed dispersal period, between October 2018 and March 2019, was 2.14 m. We used this tide line to set the "main seed dispersal area" boundary so we could focus the modeling of UAS vegetation cover data on drivers of marsh, rather than upland, vegetation colonization.

The highest elevation of newly-colonized *Salicornia* on western, initially-bare transects was marginally significantly lower than the highest elevation of existing *Salicornia* on eastern and southern transects (Fig. S4; one-tailed t-test, $p = 0.073$). Contrary to our expectation, the upper limit of newly-colonized *Salicornia* on initially-bare transects was not always below 2.14 m, the highest tide during the main seed dispersal period (Fig. S4). However, only 3% of all new marsh cover was found in quadrats above 2.14 m, and mean cover of new marsh and upland vegetation in these quadrats did not differ significantly (t-test, $p = 0.65$). This equal dominance of marsh and upland cover above 2.14 m, and the vast majority (97%) of new marsh vegetation occurring below 2.14 m, supports our decision to use the "main seed dispersal area" boundary to limit the UAS analysis of marsh vegetation colonization.

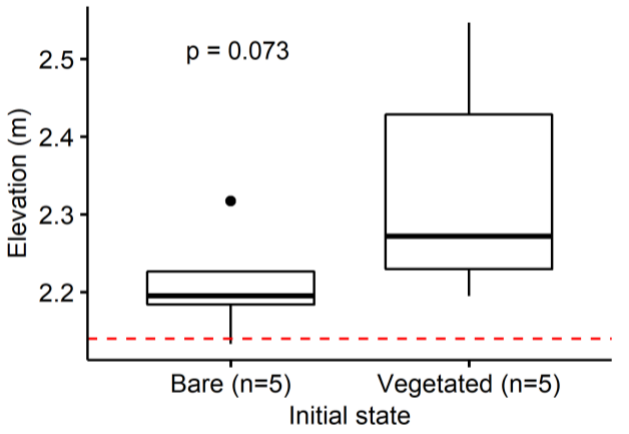

Fig. S4 Upper elevational boundary of *Salicornia* on initially-bare western transects compared with initially-vegetated eastern and southern transects, with reference to the highest tide during the high seed dispersal period between October 2018 and March 2019 (2.14 m, dashed line)

Site-Wide UAS Monitoring of Vegetation Colonization

We operated a DJI Phantom 4 Pro quadcopter drone (SZ DJI Technology Co., Ltd., Shenzhen, China) to collect red, green, and blue (RGB) data with a 20 megapixel camera and near infrared (NIR) and red-edge data with a Sentera Double 4k sensor (Sentera Inc., Minneapolis, MN). We analyzed vegetation in October 2019 imagery using only RGB data due to incomplete NIR coverage, which seemed sufficient for detecting plants due to the high resolution of the RGB imagery (pixel size = 0.79 cm). We collected October imagery under clear conditions, at a flight altitude of 30 m, with 75% frontal and 70% side overlap. We selected this flight altitude as a balance between image resolution (0.79 cm) and flight time (2.5 hours) based on prior experimentation at the site (Haskins et al. 2021). A total of 50 white, 30-cm round bucket lids were anchored to the marsh plain as ground control points (GCPs) for drone data processing. Elevation at GCPs was surveyed similarly to quadrat locations. We used DroneDeploy for flight planning and Agisoft Metashape and Sentera FieldAgent platforms for processing orthomosaics and DSMs (RMSE of DSM vertical accuracy was approximately 3 cm).

We compared two methods for classifying vegetated and unvegetated areas in October 2019 UAS imagery before selecting the final classified image for modeling UAS-derived vegetation cover. The methods we compared were a pixel-based approach with a maximum likelihood classifier and an object-based approach with a support vector machine classifier. For both classifications, we initially created three classes, and then merged the two unvegetated classes together to achieve an image of vegetation presence/absence (unvegetated mud, n = 34 training samples; unvegetated shadows, n = 9 training samples; vegetation, n = 10 training samples). While our training sample size was small, it performed better than several larger sample sizes, likely due to increased overlap between classes with the larger sample sizes tested. We used Accuracy Assessment tools in ArcGIS Pro (v. 2.3, ESRI 2019) to verify the classification method using randomly generated points independent from the training sample locations (similar to Chapple and Dronova 2017). To select segmentation parameters for the object-based classification, we used an iterative approach in ArcGIS Pro's *Image Classification Wizard* (ESRI 2019). We began with default settings and incrementally altered spectral detail by 0.5, spatial detail by 1, and minimum segment size by 1 to distinguish vegetation from mud,

prevent excess segmentation of individual plants and mud patches, and ensure that small plants were included (final segmentation parameters: spectral detail = 17.5, spatial detail = 14, minimum segment size = 12).

We assessed accuracy of the classified images in ArcGIS Pro (56 vegetated and 43 unvegetated points, "ground truthing" by visual assessment of the high-resolution imagery) and calculated the true skill statistic using the accuracy assessment confusion matrix, a measure of model performance based on true-positives and true-negative rates for each class (Allouche et al. 2006). After selecting the final classified image based on accuracy assessment and qualitative visual inspection, we categorized the cells within the main seed dispersal area (as identified by inundation data, excluding tidal creek interiors and actively planted areas) as "high" or "low" cover using the Jenks natural breaks classification method (Jenks 1967). We randomly sampled cells in the high-cover class, increasing the sample size from 150 to 300 in increments of 50, and calculated the Nearest Neighbor Index (NNI; ESRI 2019) to find the largest sample size that did not exhibit significant within-strata clustering (Clark and Evans 1954). We only calculated NNI for the high-cover cells because they appeared more susceptible to autocorrelation, and we applied the same sample size to the low-cover cells. Based on this method, we randomly sampled 150 cells in each of the two cover classes (NNI = 0.95, z = -1.12).

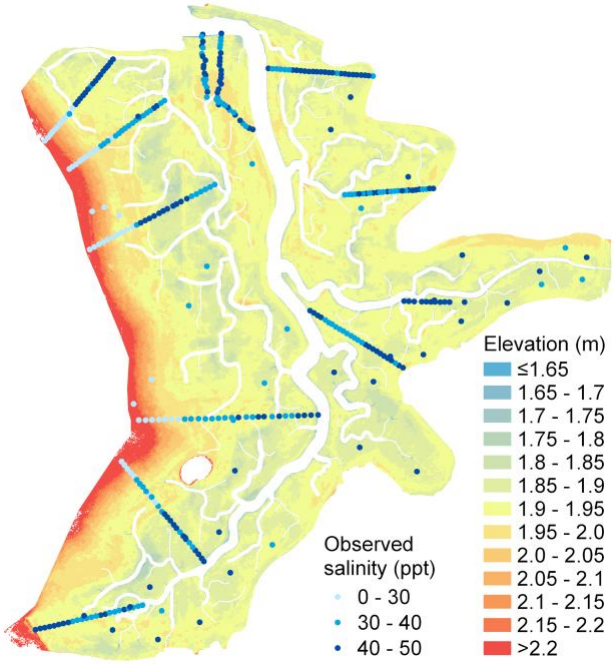

Fig. S5 UAS-derived digital surface model (DSM) of Hester Marsh in May 2019 and salinity data points collected in September 2019 (n = 349). Site-wide salinity was modeled based on these data points using May 2019 elevation, soil addition/removal amount, and tidal creek distance as predictors (out-of-bag RMSE = 3.1)

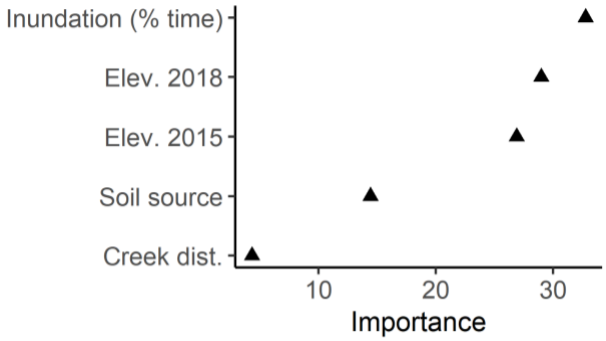

Fig. S6 Importance for variables included in the random forest model of UAS-derived classified vegetation cover in 300 plots. Variable importance is measured as percentage increase in mean squared error when the variable is randomly permuted

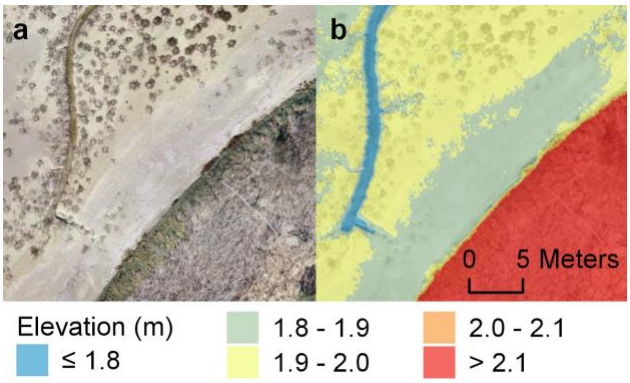

Fig. S7 Bare ground between new colonization and existing marsh vegetation outside of the construction zone on the restoration site edge in (**a**) UAS imagery (October 2019) and (**b**) semi-transparent digital surface model (May 2019) overlaid on UAS imagery. This bare strip was lower in elevation, supporting field observations of water pooling on site edges

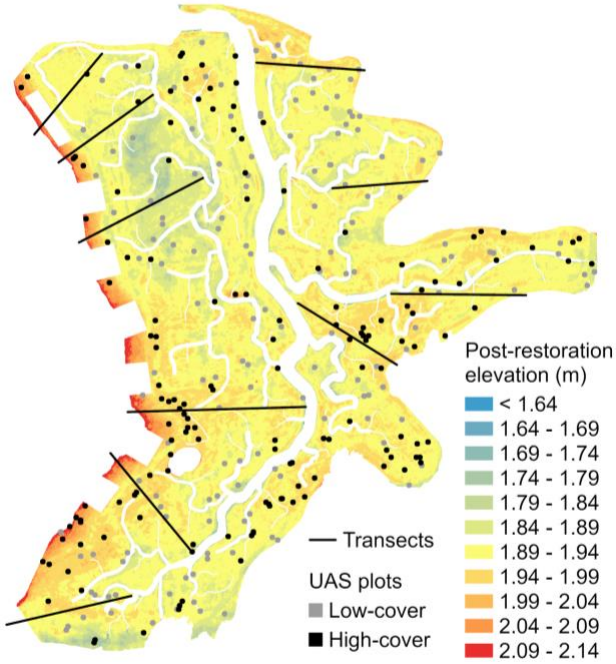

Fig. S8 Map showing locations of low-cover and high-cover UAS plots and field transects relative to elevation at Hester Marsh following soil addition (Aug 2018 DSM)

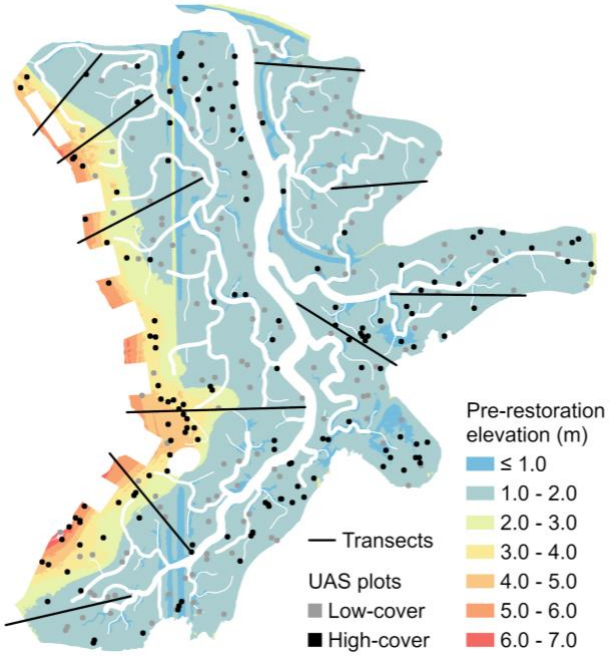

Fig. S9 Map showing locations of low-cover and high-cover UAS plots and field transects relative to elevation at Hester Marsh prior to restoration (Oct 2015 DSM)

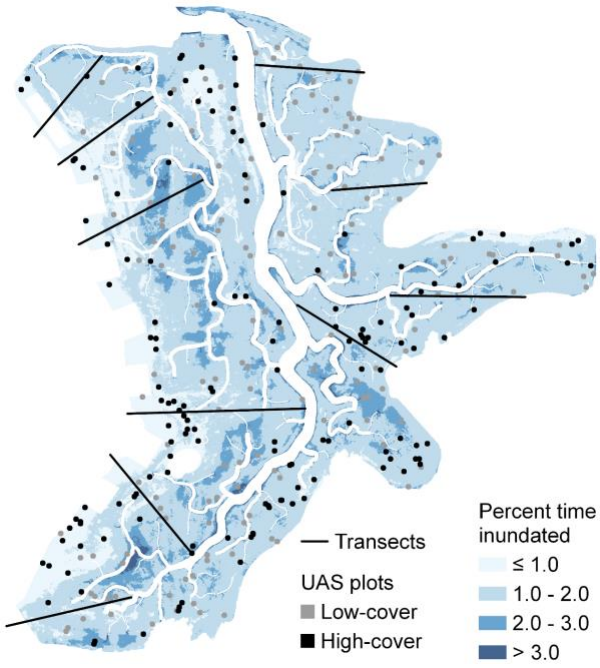

Fig. S10 Map showing locations of low-cover and high-cover UAS plots and field transects relative to inundation time (%) at Hester Marsh (tide data from Aug 2018 – May 2019, calculated based on elevations from May 2019 DSM)

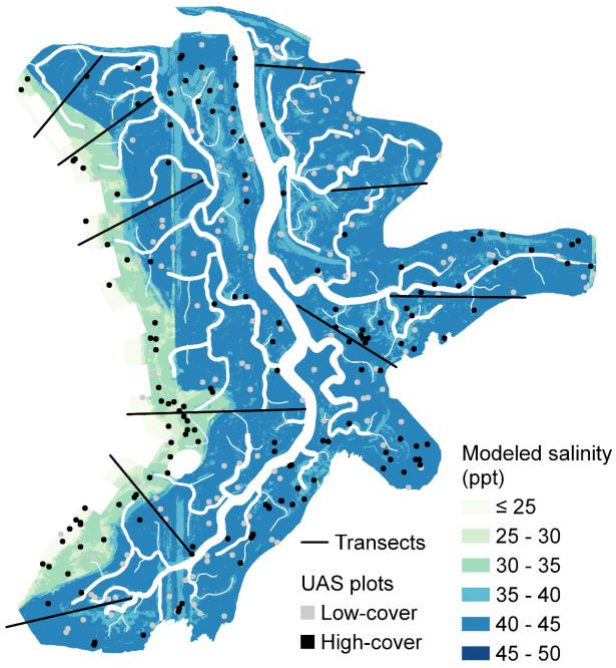

Fig. S11 Map showing locations of low-cover and high-cover UAS plots and field transects relative to modeled salinity at Hester Marsh. To model salinity, an ArcGIS Pro forest-based regression model was trained using 349 salinity data points collected in the field using a conductivity meter, with elevation (May 2019 DSM, Fig. S5), tidal creek distance (Fig. S14), and amount of soil addition or removal during construction as predictors (out-of-bag RMSE = 3.08 ppt)

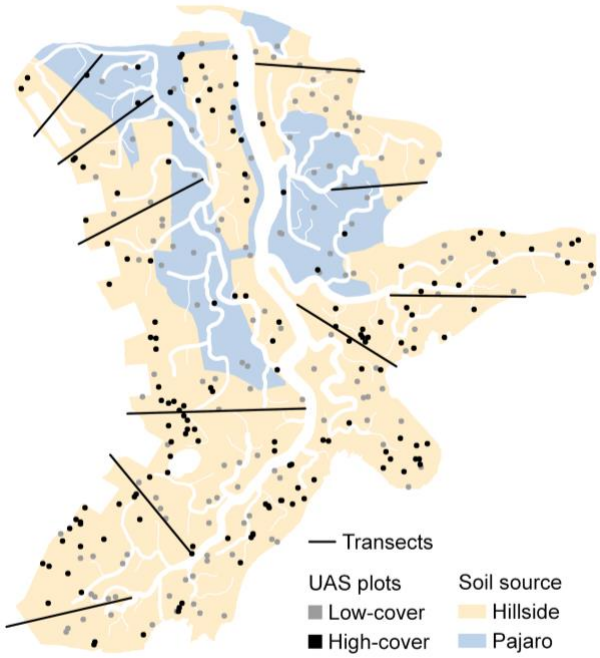

Fig. S12 Map showing locations of low-cover and high-cover UAS plots and field transects relative to areas at Hester Marsh that received soil from different sources during site construction (the adjacent hillside and a Pajaro River dredging project)

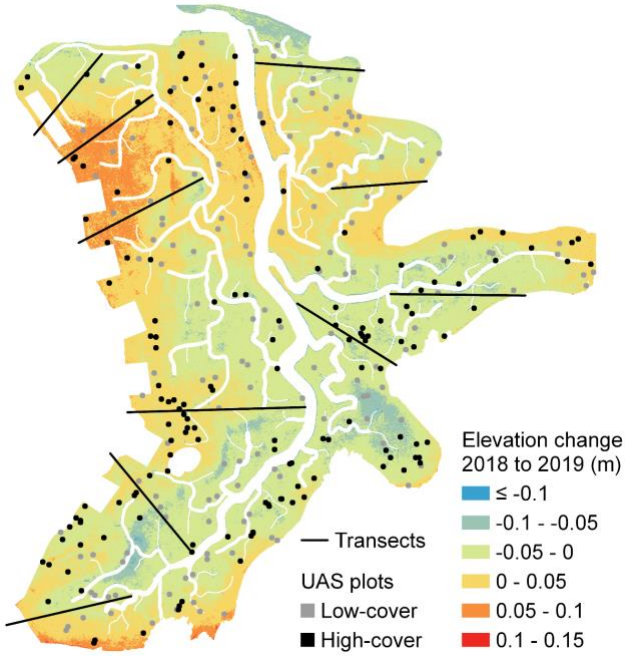

Fig. S13 Map showing locations of low-cover and high-cover UAS plots and field transects relative to elevation change over the first year of restoration at Hester Marsh (August 2018 DSM subtracted from May 2019 DSM)

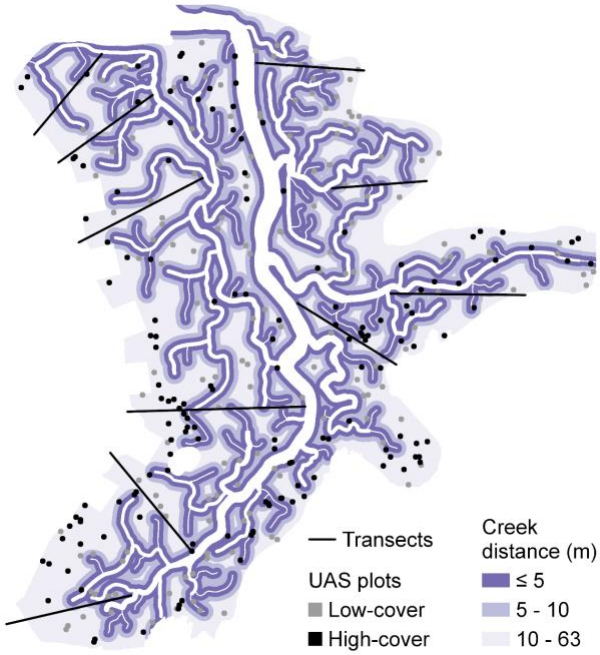

Fig. S14 Map showing distance of low-cover and high-cover UAS plots and field transects relative to tidal creeks across Hester Marsh. Calculated using Euclidean distance from tidal creek polygon feature

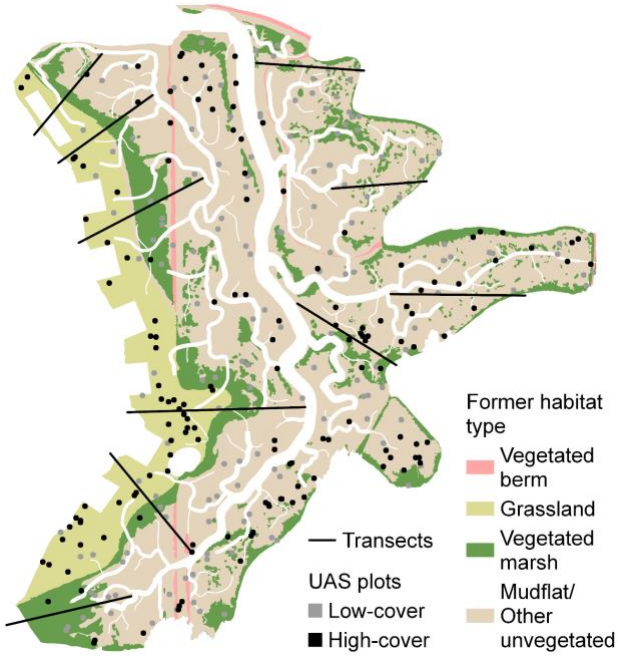

Fig. S15 Map showing locations of low-cover and high-cover UAS plots and field transects relative to habitat types across Hester Marsh in 2015, prior to restoration. Digitized from 2015 UAS imagery

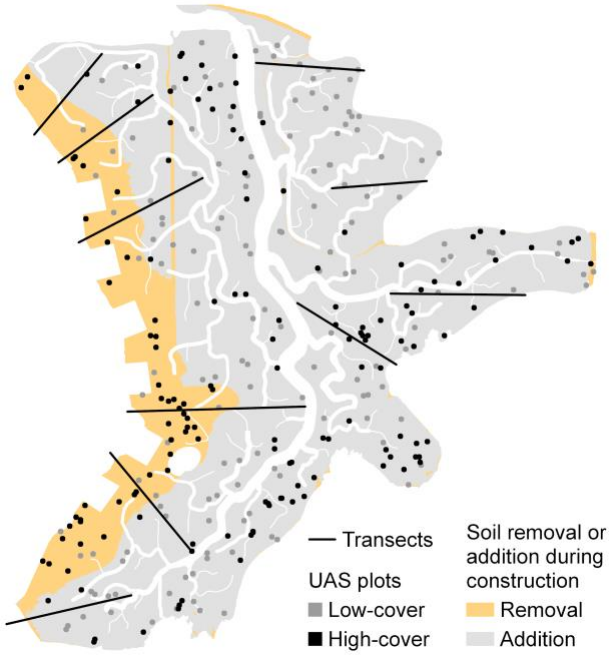

Fig. S16 Map showing locations of low-cover and high-cover UAS plots and field transects relative to soil addition versus removal areas at Hester Marsh during construction of the restoration site. Calculated by subtracting an October 2015 DSM from an August 2018 DSM

Soil Comparison at Well- and Poorly-Vegetated Sites

In selecting sites for soil comparison, we held elevation and creek distance relatively constant because other marsh restoration research suggests these are two important factors influencing vegetation colonization and growth (Mayer 1987; Chapple and Dronova 2017), and we wanted to focus on sediment properties that might contribute to the patterns emerging at Hester Marsh during the first year of restoration. We used GIS layers to select sampling sites, first by limiting the elevation range to 1.88 m to 1.95 m (using an August 2019 DSM, pixel size = 2.6 cm) and then by selecting representative well-vegetated and poorly-vegetated areas through visual inspection of high-resolution true color drone imagery from August 2019 (pixel size = 1.3 cm). We used imagery to ensure that DSM values were representing elevations of the bare ground. After selecting a general representative area within the elevation range, we created a point approximately 10 m from a tidal creek, and used a GPS to navigate to this point in the field.

We conducted grain size analysis of both bulk soil (including organic material) and digested soil (dissolved with acetic acid and hydrogen peroxide to remove organic material) using a laser particle size analyzer (D.W. Clarke et al. 2014). We calculated moisture content by calculating the difference in the sample weight of the wet core and the weight of the same sample after baking for 24 hours in a convection oven at 60 degrees Celsius. After removing moisture, we measured organic carbon content using a muffle furnace according to methods described by the National Lacustrine Core Facility (2013). We heated soil at 550 degrees Celsius for four hours to remove organic carbon content, and at 1100 degrees Celsius for two hours to remove carbonates. We examined Atterberg liquid limits (the moisture content at the boundary between liquid and plastic states) using a mechanical liquid limit device and plastic limits (the moisture content and the boundary between plastic and semisolid states) by rolling out samples

according to New York Department of Transportation, Geotechnical Engineering Bureau methods (2015).

The following parameters were analyzed by Control Laboratories (Watsonville, CA, USA; M. Galloway, personal communication, October 15, 2020): nitrate, ammonium, phosphorus, saturation (%), pH, conductivity, sodium, chloride, sulfate, calcium, potassium, magnesium, and cation exchange capacity. Nitrate and ammonium were extracted from the soil samples using a 2N potassium chloride (KCl) solution with a ratio of 1 part soil to 5 parts KCl. After shaking for 20 minutes and filtering, nitrate and ammonium concentrations were analyzed colorimetrically on a flow injection analyzer. Phosphorus was extracted by Olsen Bicarbonate Extraction for 30 minutes using a ratio of 1 part soil to 20 parts extract. After filtering, phosphorus concentration was analyzed manually by colorimetric method. Saturation was measured as the percentage of water added to the dry soil sample to make a saturation paste. The saturation paste was used to measure pH. Conductivity was measured for the saturation paste extract. Chloride and sulfate were quantified by analyzing the saturation paste extract using ion chromatography for anions. Exchangeable calcium, magnesium, sodium, and potassium were extracted with 1N ammonium acetate using a ratio of 1 part soil to 10 parts extract. After shaking for 20 minutes and filtering, exchangeable cations were analyzed using inductively coupled plasma atomic emission spectrometry (ICP-AES). Cation exchange capacity was calculated by summing exchangeable cations (calcium, magnesium, sodium, potassium).

Because soil source was a moderately important factor in vegetation modeling, we compared the lab-measured soil properties and field-collected conductivity/salinity data between areas that received Pajaro River dredge material during construction and those that received hillside material to identify differences that might have affected vegetation colonization (soil source areas in Fig. S12). Of the 20 sites where we collected soil samples, only three sites likely represented Pajaro source material and all were classified as “poorly-vegetated” sites, so we compared these samples only with the other samples within the poorly-vegetated category. We examined differences between the sites representing different soil sources using two-tailed t-tests for each of the variables that emerged as important in the SIMPER analysis (Table S1). While our sample size was very small for this comparison ($n = 3$ and 7 for Pajaro and hillside soil sites, respectively), sites with hillside material had significantly greater moisture content ($p = 0.044$), larger mean bulk grain size ($p = 0.029$), and lower lab-measured conductivity ($p = 0.028$). We also examined salinity in relation to soil source, modeled from field conductivity measurements along the 10 transects, considering only the soil addition areas because salinity modeling indicated lower salinity in areas where soil was scraped. Based on these data, salinity was significantly lower on hillside soil areas (two-tailed t-test, $p = 0.018$, $df = 71$), though the difference in mean salinity was only 1.0 ppt.

Table S1. Comparison of soil properties between well- and poorly-vegetated sites in October 2019 (n = 20). The Variable column lists the top 14 factors identified as contributing to the separation of the two groups in a SIMPER analysis, and the % Contribution column shows how much each factor contributes to this separation. The mean and standard deviation for each factor are shown for poorly-vegetated and well-vegetated sites, with p-values for two-tailed t-tests between groups.

		Poorly-vegetated		Well-vegetated		
Variable	**% Contribution**	**Mean**	**SD**	**Mean**	**SD**	**P-value**
Ammonium (ppm)	4.92	3.05	0.93	2.23	0.34	p = 0.023
Chloride (meq/l)	4.86	1611.0	131.6	1374.3	255.5	p = 0.021
Conductivity (dS/m)	4.81	102.6	8.2	91.6	11.1	p = 0.022
Sodium (ppm)	4.76	14154.0	1577.2	11786.6	2648.6	p = 0.029
Atterberg liquid limit (%)	4.42	20.8	3.8	24.9	5.9	p = 0.084
Cation exchange capacity (meq/100 g)	4.38	91.9	11.2	79.1	19.8	p = 0.098
Moisture content (%)	4.37	15.3	4.6	19.4	5.9	p = 0.099
Sulfate (meq/l)	4.19	158.5	20.5	142.2	30.3	p = 0.18
pH SMP buffer	4.18	7.61	0.06	7.56	0.08	p = 0.18
Bulk grain size (μm)	4.18	3.28	0.81	3.91	1.22	p = 0.19
Potassium (ppm)	4.10	461.1	44.3	414.9	114.2	p = 0.26
pH sample	4.08	7.10	0.21	6.95	0.37	p = 0.29
Saturation (%)	4.03	38.1	2.6	39.9	5.2	p = 0.34
Magnesium (ppm)	3.97	2442.0	360.8	2220.3	715.7	p = 0.40

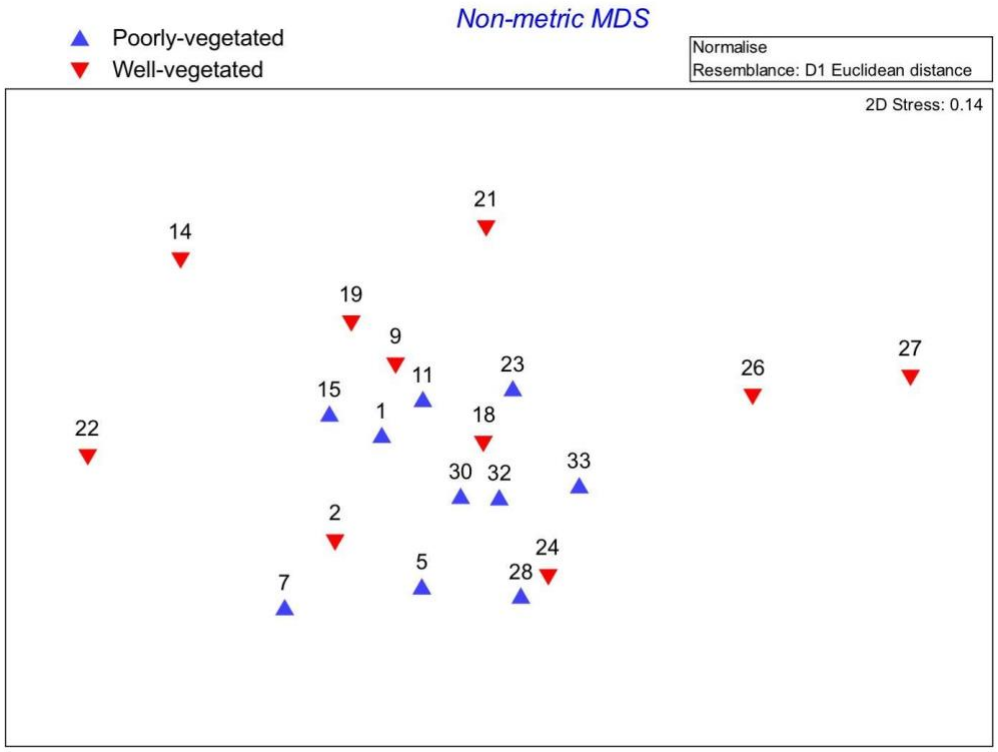

Fig. S17 Non-metric multidimensional scaling results for soil samples collected at well- and poorly-vegetated sites in October 2019 (n = 20)

References

Allouche, O., A. Tsoar, and R. Kadmon. 2006. Assessing the accuracy of species distribution models: Prevalence, kappa and the true skill statistic (TSS). *Journal of Applied Ecology* 43: 1223–1232.

Chapple, D., and I. Dronova. 2017. Vegetation Development in a Tidal Marsh Restoration Project during a Historic Drought: A Remote Sensing Approach. *Frontiers in Marine Science* 4.

Clark, P.J., and F.C. Evans. 1954. Distance to Nearest Neighbor as a Measure of Spatial Relationships in Populations. *Ecology* 35(4): 445–453.

Clarke, D.W., J.F. Boyle, J. Lario, and A.J. Plater. 2014. Meso-scale barrier estuary disturbance, response and recovery behaviour: Evidence of system equilibrium and resilience from high-resolution particle size analysis. *The Holocene* 24(3): 357–369.

Haskins, J., C. Endris, A.S. Thomsen, F. Gerbl, M.C. Fountain, and K. Wasson. 2021. UAV to Inform Restoration: A Case Study From a California Tidal Marsh. *Frontiers in Environmental Science* 9(642906): 1–20.

Huiskes, A.H.L., B.P. Koutstaal, P.M.J. Herman, W.G. Beeftink, M.M. Markusse, and W. De Munck. 1995. Seed Dispersal of Halophytes in Tidal Salt Marshes. *Journal of Ecology* 83(4): 559–567.

Jenks, G.F. 1967. The data model concept in statistical mapping. *International yearbook of cartography* 7(1): 186–190.

Mayer, M.A. 1987. Flowering plant recruitment into a newly restored salt marsh in Elkhorn Slough, California. Moss Landing Marine Laboratories.

Morzaria-Luna, H.N., and J.B. Zedler. 2007. Does seed availability limit plant establishment during salt marsh restoration? *Estuaries and Coasts* 30(1): 12–25.

National Lacustrine Core Facility. Loss-on-Ignition Standard Operating Procedure. 2013. LacCore, National Lacustrine Core Facility. http://lrc.geo.umn.edu/laccore/assets/pdf/sops/loi.pdf. Accessed 20 July 2020.

Noe, G.B., and J.B. Zedler. 2001. Variable rainfall limits the germination of upper intertidal marsh plants in southern California. *Estuaries* 24(1): 30–40.

[NYDOT] State of New York Department of Transportation. Geotechnical Test Method: Test Method for Liquid Limit, Plastic Limit, and Plasticity Index. GTM-7 Revision #2. 2015. State of New York Department of Transportation, Geotechnical Engineering Bureau. https://www.dot.ny.gov/divisions/engineering/technical-services/technical-services-repository/GTM-7b.pdf. Accessed 20 July 2020.